

In these conditions, one obtains after simple but lengthy algebra

$$v/f = f'/f = (K_F \Sigma_F \tau_R / K_{F'} \Sigma_{V'} \tau_I)^{1/2}$$

for any value of the illumination time after the initial transient. The situation is, therefore, similar to that found under irradiation. During an interrup-

tion, anion vacancies are lost by trapping, and consequently, on resuming illumination, a new equilibrium is reached with the same value for the ratio v/f but a lower concentration of vacancies (filled or not). It follows immediately that $\Delta v \sim \Delta f$, relating the change in vacancy concentration during the dark time to the fast decrease in F -center concentration upon resumption of the illumination.

- ¹F. Agulló-López, *Solid State Commun.* **4**, 275 (1966).
²C. Sánchez and F. Agulló-López, *Solid State Commun.* **5**, 494 (1967).
³C. Sánchez and F. Agulló-López, *Phys. Status Solidi* **29**, 217 (1968).
⁴R. T. Platt and J. J. Markham, *Phys. Rev.* **92**, 1 (1953).
⁵C. Z. Van Doorn, *Philips Res. Rept. Suppl.* **4**, 1 (1962).
⁶N. Itoh and T. Suita, *J. Phys. Soc. Japan* **18**, Suppl. III, 340 (1963).
⁷R. Onaka, A. Fujita, and A. Fukuda, *J. Phys. Soc. Japan* **18**, Suppl. II, 263 (1963).
⁸H. Rabin, *Phys. Rev.* **129**, 129 (1963).
⁹C. T. Butler, *Phys. Rev.* **141**, 750 (1966).
¹⁰M. Hirai and A. B. Scott, *J. Chem. Phys.* **46**, 2896 (1967).
¹¹R. A. Andrews and Y. W. Kim, *Phys. Rev.* **170**, 793 (1968).
¹²A. Kikudi and K. Ozawa, *Proceedings of the International Meeting on Color Centers in Alkali Halides*, Rome, 1968 (unpublished).
¹³I. Schneider and C. E. Bailey, *Solid State Commun.* **7**, 657 (1969).
¹⁴G. Giuliani, *J. Phys. Chem. Solids* **30**, 217 (1969).
¹⁵Throughout this paper, V will refer to a free-anion vacancy.
¹⁶H. Pick, *Ann. Physik* **31**, 365 (1938).
¹⁷W. D. Compton and H. Rabin, in *Solid State Physics*, edited by F. Seitz and D. Turnbull (Academic, New York, 1964), Vol. 16, pp. 121-226.
¹⁸C. J. Delbecq, P. Pringsheim, and P. Yuster, *J. Chem. Phys.* **19**, 574 (1951).
¹⁹F. Luty, *Z. Physik* **165**, 17 (1961).
²⁰F. J. Dudek and L. I. Grossweiner, *J. Phys. Chem. Solids* **30**, 2030 (1969).
²¹P. Scaramelli, *Nuovo Cimento XLV B*, 119 (1966); R. Fieschi, M. Golo, and P. Scaramelli, *International Conference on Luminescence*, Budapest, 1966 (unpublished), Vol. 1, p. 86.
²²M. Tomura, K. Murase, M. Takebayashi, and T. Kitada, *J. Phys. Soc. Japan* **19**, 1991 (1964).
²³T. Kitada, Y. Kakui, and M. Tomura, *J. Phys. Soc. Japan* **25**, 915 (1968).
²⁴C. J. Delbecq, *Z. Physik* **171**, 560 (1963).
²⁵The low intensity of the F' band, during or after irradiation, prevented our paying attention to it in our previous work on anomalous F coloring after interruptions (Refs. 3 and 26). We are indebted to Dr. Capelletti (Parma) for first pointing out this to us.
²⁶C. Sanchez and F. Agulló-López, *Cryst. Lattice Def.* **1**, 109 (1969).

Infrared Study of the Lattice Vibrations in LiTaO_3

A. S. Barker, Jr., A. A. Ballman, and J. A. Ditzenberger

Bell Telephone Laboratories, Murray Hill, New Jersey 07974

(Received 25 May 1970)

Polarized infrared reflectivity measurements have been made on single-crystal LiTaO_3 in the frequency range $20 - 10\,000\text{ cm}^{-1}$ at $300\text{ }^\circ\text{K}$. Kramers-Kronig and classical-oscillator dispersion-theory analyses of these data have yielded values for the frequency, strength, and linewidth of the infrared-active transverse optic modes and longitudinal optic modes. Analysis of the far-infrared interference spectrum yields values of 41 and 40 for the ordinary and extraordinary clamped dielectric constants, as well as values for their temperature dependence and dispersion. A calculation is made of the spontaneous polarization in LiTaO_3 and LiNbO_3 using the x-ray ion displacements.

I. INTRODUCTION

LiTaO_3 is an optically uniaxial trigonal crystal belonging to the point group $3m$. It was found to be ferroelectric by Matthias and Remeika¹ and to ex-

hibit large electrooptic effects by Lenzo *et al.*² The ferroelectric transition temperature is approximately $900\text{ }^\circ\text{K}$. With the production of high-quality single crystals of LiTaO_3 ,³ there has been increased interest in the material for use in

nonlinear optical experiments as well as for electro-optic device applications.⁴ Detailed x-ray diffraction⁵ and neutron diffraction⁶ studies show LiTaO₃ to have the same crystal structure as LiNbO₃. The present work parallels an earlier infrared study of LiNbO₃.⁷ In that study the symmetry types of the vibrational modes and the mode softening (i. e., vibrational frequency approaching zero) at the ferroelectric phase transition were analyzed theoretically and experimentally. Most of that analysis applies here and will be referred to where appropriate. The main results of the present work are the reflectivity spectra which allow assignment of strengths and frequencies to most of the polar vibrational modes predicted by group theory. The strongest modes produce considerable dispersion and absorption of the dielectric constant in the far infrared. These effects have been measured separately using transmission spectroscopy and yield, along with other quantities, the clamped dielectric constants.

II. EXPERIMENTAL PROCEDURE AND DATA ANALYSIS

The samples of LiTaO₃ used for this experiment were grown from a melt using the Czochralski pulling technique.³ The boule was electrically poled just below the ferroelectric transition temperature to create a single-domain sample.⁸ A rectangular shaped slab 0.3 × 1.6 × 1.2 cm, having the *c* axis perpendicular to its long dimension was cut from the center of the boule, lapped, and then polished with 1- μ diamond compound. Polarized reflectivity measurements with the electric vector perpendicular and then parallel to the *c* axis ($\vec{E} \perp c$ and $\vec{E} \parallel c$) were made in the wavelength region 5–200 μ using methods described in earlier work.⁹ Two other samples of LiTaO₃ were lapped down to a thickness of 30 and 147 μ for transmission measurements below 90 cm⁻¹ using a far infrared Michelson interferometer.

A Kramers-Kronig analysis of the reflectivity data was made for each polarization to obtain the real and imaginary parts of the dielectric function ϵ . From the plot of the imaginary part (ϵ'') of the dielectric function versus frequency, the parameters of the transverse-optic (TO) infrared-active phonon modes can be estimated. Using such estimates for the values of frequency, strength, and linewidth, fits to reflectivity were carried out using an expansion of the dielectric function in a sum of classical-oscillator terms:

$$\epsilon = \epsilon_{\infty} + \sum_j \frac{S_j \omega_j^2}{\omega_j^2 - \omega^2 - i\omega\gamma_j} \quad (1)$$

This procedure is explained in detail by Spitzer and Kleinman⁹ and has been used for LiNbO₃.⁷ By varying the parameters of each oscillator to obtain the best fit of theory to the reflectivity data, we ob-

tain more accurate values of the TO-mode parameters ω_j , S_j , and γ_j than could be estimated from the original Kramers-Kronig analysis. A similar expansion of $1/\epsilon$ could be carried out¹⁰ to obtain the longitudinal-optic (LO) mode parameters by accurate fits to the reflectivity. There is generally less interest in the LO modes because they do not contribute directly to infrared absorption, so we quote the LO frequencies obtained from the oscillator expansion of ϵ .⁷

At high frequencies (above 500 cm⁻¹), the reflectivity flattens out and the Kramers-Kronig analysis suggests that $\epsilon(\perp)$ and $\epsilon(\parallel)$ both approach 4.5. Accurate refractive index data¹¹ show that the index $n = \sqrt{\epsilon}$ is slightly anisotropic (less than 0.5%) and does not flatten but rises rapidly in the visible due to electronic resonances. We have analyzed the published index curves¹¹ to derive ϵ_{∞} , the effective high-frequency dielectric constant, as was done previously for LiNbO₃.⁷ At frequencies below all optical phonons, but well above any piezoelectric resonances, the dielectric function is again fairly flat. This clamped dielectric constant, usually denoted ϵ_0 , is obtained from the oscillator-fit procedure by taking the sum of ϵ_{∞} plus all mode strengths used to fit the reflectivity spectrum.⁹

Transmission measurements made on the thin samples of LiTaO₃ showed interference peaks. Fits to the transmission spectra using standard interference formulas were used to obtain the attenuation at very low frequencies. In addition these fits were used to predict more accurate values of ϵ_0 using the interference peaks and an accurate measurement of sample thickness.

III. RESULT AND DISCUSSION

A. Optic Modes

Figures 1 and 2 show the reflectivity data for each polarization. The bottom of each figure shows the plots of the imaginary part of the dielectric constant $\text{Im}(\epsilon)$ and $\text{Im}(-1/\epsilon)$ obtained from the Kramers-Kronig analysis of the reflectivity data. Peaks in $\text{Im}(\epsilon)$ correspond to TO modes and peaks in $\text{Im}(-1/\epsilon)$ correspond to LO modes. As discussed above, fits to the reflectivity were carried out to obtain accurate mode parameters. Tables I and II show the mode parameters. The tables show also the values of ϵ_{∞} determined by analysis of the index of refraction. As in LiNbO₃, we expect nine transverse and nine longitudinal *E* symmetry ($\vec{E} \perp c$ axis) fundamental modes.⁷ The $\text{Im}(\epsilon)$ spectrum shows only six strong TO modes, but the (some quite weak) or even more, depending on how accurately the reflectivity must be fit. Because of this discrepancy in the number of modes observed, a separate discussion is given below of the mode assignments and several comparisons are made with the Raman spectra of Kaminow and Johnston^{12,13}

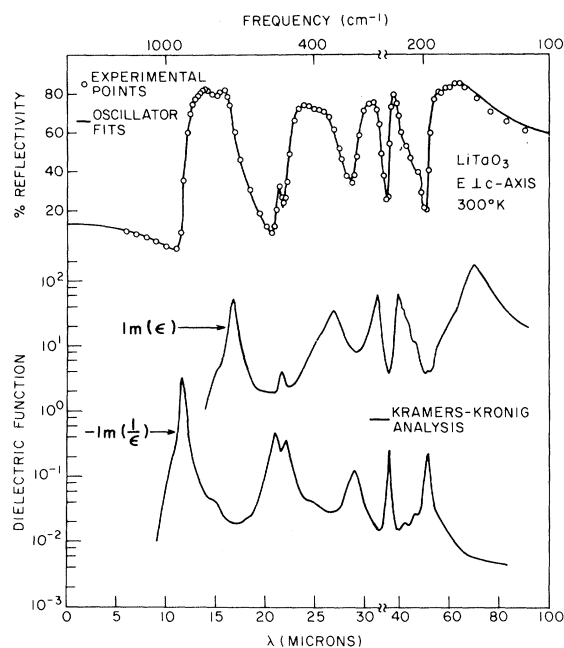


FIG. 1. Reflectivity and dielectric functions for E symmetry modes of LiTaO_3 . The parameters associated with the solid curve at the top are listed in Table I.

(KJ). For $\vec{E} \parallel c$ axis (A_1 -type modes), group theory predicts four TO and four LO modes.⁷ Table II lists three strong TO modes and two weak modes. The discussion given below suggests that only three of these modes are fundamental lattice vibrations.

In Tables I and II, TO-mode frequencies are generally precise to better than one-fifth of the linewidth quoted. The LO frequencies corresponding to main peaks in $\text{Im}(-1/\epsilon)$ have the same accuracy where the appropriate linewidth is that shown in the $\text{Im}(-1/\epsilon)$ spectra in Fig. 1 or 2. The frequencies of other LO modes have a precision which may be less than that of the stronger modes but which can only be quoted by making a separate study of the effects of the mode on the reflectivity spectrum.

$\vec{E} \parallel c$ Axis Mode Assignments

There are four A_1 -type vibrations expected on the basis of group theory.⁷ These modes are all both Raman and infrared active. These vibrations are split into four pairs of TO and LO modes. To shorten the discussion we will consider only the TO modes. $\text{Im}(\epsilon)$ (Fig. 2) shows three main peaks plus weak fine structure. KJ find these same peaks as prominent features in the Raman spectrum.^{12,13} Comparisons with the corresponding Raman spectra of LiNbO_3 ^{7,12,13} leave little doubt that these TO modes at 200, 357, and 596 cm^{-1} are fundamentals. For the fourth mode we must choose between 253-cm^{-1} Raman mode seen by KJ or the fairly strong 657-cm^{-1} infrared mode which caused a prominent dip in re-

fectivity (Fig. 2). The reasonably large infrared strength of the 657 mode and its presence (at 648 cm^{-1}) in the Raman spectra suggests that it is fundamental. Many oxides, however, show extra spurious modes on the top of reststrahlen bands very similar to the 657 mode here.^{9,14,15} To test the 253-cm^{-1} mode reported by KJ, we have inserted this mode in our oscillator fit to the reflectivity. The measured reflectivity rules out a mode with exactly the parameters quoted by KJ but there is enough structure in the reflectivity to suggest the presence of a mode at 241 cm^{-1} . Figure 3 shows the test fit. This frequency difference ($241\text{--}253\text{ cm}^{-1}$) is within the joint uncertainties of the infrared and Raman methods. From the above considerations (see also the arguments by KJ) we conclude that the fundamental TO modes are at 200, 241, 357, and 596 cm^{-1} at 300°K . The four associated LO modes may be found by standard methods.

$\vec{E} \perp c$ Axis Mode Assignments

In Fig. 1, the $\text{Im}(\epsilon)$ spectrum shows six strong well-resolved E -type modes. These modes at 142, 253, 316, 375, 462, and 594 cm^{-1} are fundamentals and agree with the assignments of KJ. In addition, there is considerable fine structure which we have approximated by seven additional modes. Most of these additional modes are stronger than the 462-cm^{-1} fundamental, but they have a much smaller effect on the reflectivity because of being near other

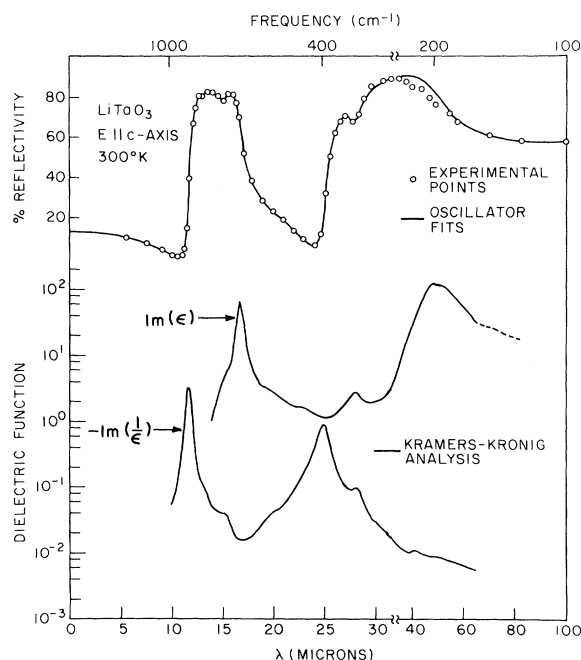


FIG. 2. Reflectivity and dielectric functions for A_1 symmetry modes of LiTaO_3 . See Table II for the oscillator-fit parameters.

TABLE I. E symmetry mode parameters determined by oscillator fits to the reflectivity.

LiTaO ₃ frequency (cm ⁻¹)	Polarization	Optic modes S_j	$\vec{E} \perp c$ axis γ_j (cm ⁻¹)
142	T	24.1	14
(165) ^a	L, T	0.8	11
(175)	L, T	0.24	7
192	L
(215)	T, L	0.36	13
(238)	T, L	2.0	19
253	T	2.4	9
278	L
316	T	2.5	14
345	L
375	T	2.0	26
(405)	L, T	0.15	24
455	L
462	T	0.036	6
474	L
594	T	2.33	32
(673)	L, T	0.05	34
(750)	L, T	0.002	22
855	L
$\epsilon_\infty = 4.497 \pm 0.003$		$\epsilon_0 = \epsilon_\infty + \sum_j S_j = 41.5$	
ϵ_0 (from interference spectrum)			
300 °K		41.1 ± 0.25	
80 °K		39.4 ± 0.25	
15 °K		39.2 ± 0.25	

^a Bracketed modes are very weak in reflectivity. For such weak modes the transverse-longitudinal splitting is much smaller than the linewidth and we list only one frequency for both.

strong modes. We now must assign three additional TO fundamentals. KJ suggest that there is a fundamental at 206 cm⁻¹. This is consistent with our 215-cm⁻¹ mode. KJ suggest also that there is a fundamental at 662 cm⁻¹. This mode is seen in our spectra at 673 cm⁻¹ and is very similar to the A_1 mode at 657, which we concluded was not a fundamental. The 673-cm⁻¹ mode is seven times weaker than the 657 mode; thus we suspect that it is not a fundamental. Finally, KJ detect a TO mode at 74 cm⁻¹. They find an LO component at about 80 cm⁻¹. This 6-cm⁻¹ splitting corresponds to the TO mode having a strength of $S = 6$. We have made a careful study of the reflectivity near 80 cm⁻¹ and find no mode structure. A study of fits to the reflectivity shows that our reflectivity uncertainties would allow a mode of strength at most $S = 3$ (i.e., $\omega_T - \omega_L$ splitting at most 3 cm⁻¹). Since we are short of fundamentals, it was felt necessary to examine this low-frequency region in a different manner. A transmission study was made on a sample of LiTaO₃ 33 μ thick in the range 70–90 cm⁻¹. The absorption is found to rise smoothly with frequency (Fig. 4). Oscillator fits to this absorption were carried out which showed that any mode near 74 cm⁻¹ must have a strength less than $S = 1.0$ or else have a

TABLE II. A_1 symmetry mode parameters determined by oscillator fits to the reflectivity.

LiTaO ₃ frequency (cm ⁻¹)	Optics modes Polarization	$\vec{E} \parallel c$ axis S_j	γ_j
200	T ^a	30.0	28
345	L
357	T	0.005	11
388	L
596	T	2.66	18
625	L
657	T	0.34	56
(760) ^b	L, T	0.02	44
862	L
$\epsilon_\infty = 4.527 \pm 0.004$		$\epsilon_0 = \epsilon_\infty + \sum_j S_j = 37.6$	
ϵ_0 (from interference spectra)			
300 °K		39.8 ± 0.5	
80 °K		34.1 ± 0.25	
15 °K		33.5 ± 0.25	

^aA small dip in the spectra suggests another mode pair near 241 cm⁻¹ (see Sec. III A).

^bSee Ref. a in Table I.

linewidth considerably greater than that measured by KJ.

KJ have listed nine TO modes for $\vec{E} \perp c$ axis. We cannot support two of their modes (74 and 662 cm⁻¹) and are thus two modes short in assigning fundamentals. The reflectivity spectra suggest that the two remaining modes may be at 165 and 238 cm⁻¹. These are weak features, however, and their assignment as fundamentals must be regarded as tentative.

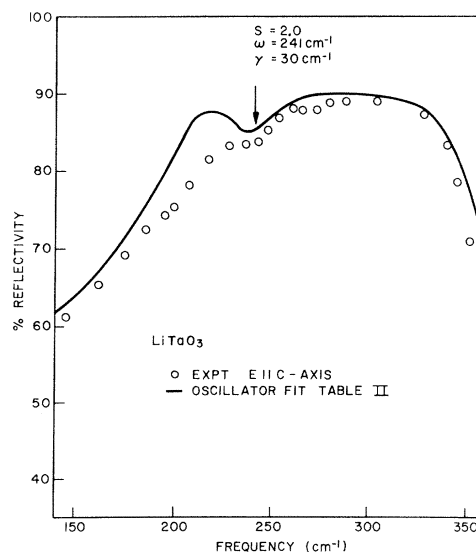


FIG. 3. Reflectivity of LiTaO₃ near 250 cm⁻¹. The solid curve results from the oscillator modes in Table II plus the additional mode at 241 cm⁻¹ listed in the figure. The reflectivity points show some evidence for such a mode.

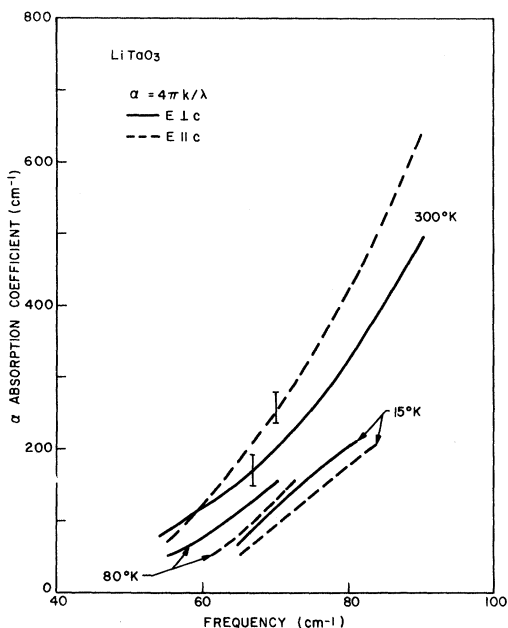


FIG. 4. Absorption coefficient in LiTaO₃ at three temperatures. The spectral resolution is 4 cm⁻¹ or better.

B. Low-Frequency Index and Absorption

Figure 4 shows the results for the attenuation coefficient α . The attenuation is similar to that measured in LiNbO₃,¹⁶ with the exception that $\alpha(\parallel)$ is about 2.5 times larger. This latter result is consistent with the fact that the lowest-frequency TO mode is much stronger in LiTaO₃ than in LiNbO₃. Cooling lowers the attenuation somewhat, but even at 15 °K the attenuation remains quite large.

Bosomworth has noted that α is roughly proportional to frequency squared in LiNbO₃.¹⁶ It is useful to note that $\alpha \sim \omega^2$ is exactly the prediction of the classical-oscillator model [Eq. (1)] at frequencies well below all optic modes. We find that Eq. (1) will fit the measured attenuation in LiTaO₃ and LiNbO₃ only if the linewidths used for the lowest TO modes are two to three times larger than the values suggested by the reflectivity fits (Tables I and II) or by the Raman linewidths. Table III gives the oscillator parameters for the lowest-frequency modes in LiTaO₃ and in LiNbO₃ which reproduce the measured attenuation below 90 cm⁻¹.

Figure 5(a) shows a typical interferogram¹⁷ for a thin plate of LiTaO₃. Figure 5(b) shows the transmission spectrum obtained by Fourier analysis of the interferogram. The well-resolved interference maxima and minima have been analyzed to give the index shown in Fig. 5(c). Also shown are the results for other temperatures and for the $\vec{E} \parallel c$ -axis polarization. The dispersion in the index fits that predicted by the lowest mode given in Tables I and II. The limiting value of ϵ_0 , however, is slightly

TABLE III. Oscillator parameters which approximately fit low-frequency absorption spectra.

LiTaO ₃				
Temp. (°K)	Polarization	S	ω (cm ⁻¹)	γ (cm ⁻¹)
300	$E \perp c$	24	142	50
300	\parallel	30	200	84
80	\perp	24	142	36
80	\parallel	30	200	40
LiNbO ₃				
300	\perp	22	152	40
300	\parallel	16	248	62
80	\perp	22	152	22
80	\parallel	16	248	25

different, and since it is obtained more reliably from the interference spectra we list it separately at the bottom of Tables I and II. The value of ϵ_0 for $\vec{E} \parallel c$ axis has been uncertain, literature values ranging from 36.2 to 43 at 300 °K. The interference method is capable of better accuracy than many of the methods used previously. In spite of rather large absorption for this particular temperature and polarization, we are able to establish that $\epsilon_0(\parallel) = 39.8 \pm 0.5$ at 300 °K.

C. Spontaneous Polarization of LiTaO₃ and LiNbO₃

X-ray studies of LiNbO₃ and LiTaO₃ have established the distortions (ion motions) which occur on cooling into the ferroelectric phase.^{5,6} In an earlier paper, these distortions were combined with estimated charges for the ions to give the spontaneous polarization P_s of the ferroelectric phase of LiNbO₃.⁷ Since that estimate was made, methods have been developed for measuring P_s and the estimate proved to be quite close.¹⁸ We now make a similar calculation for LiTaO₃ using estimated charges and a second calculation using charges derived from the mode strength. Since the polarization develops along the c axis, we need use only the y component of the distortions. The effective charge is a tensor, in general, and must have different components for the different ions in the unit cell. Only the components of effective charge appropriate to a mode of A_{2u} symmetry can be evaluated. It is noteworthy that in lattice dynamics the charge which is measured is the charge which moves when an ion moves. This must not be confused with the static point charge assumed to reside on an ion when electric field gradients are analyzed by nuclear magnetic resonance. In many materials these latter charges are much smaller than the long-wavelength lattice-dynamical charges.

Table IV lists the ion distortions. Since the distortions are related to the soft optic mode in the

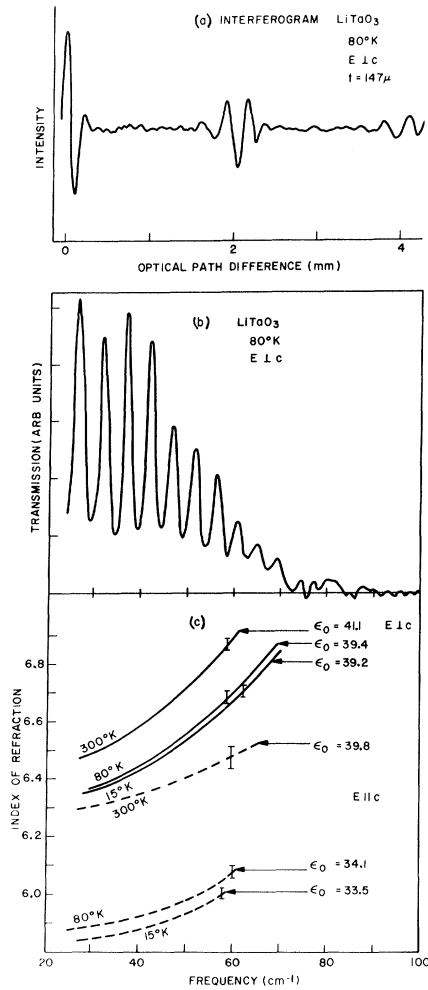


FIG. 5. (a) Interferogram of a LiTaO_3 plate at 80°K . The structure at 2 and 4 mm is characteristic of a strong channel spectrum. (b) Channel spectrum obtained by a Fourier transform of the interferogram above. (c) Index of refraction obtained for different temperatures and polarizations by analyzing channel spectra like that shown in (b).

paraelectric phase,^{7,19} (above T_c) it is of interest to go to c. m. coordinates so that the ion motions correspond to an optic-mode eigenvector. Table IV shows the eigenvector. We first use the displacements and the full formal valence charges shown in Table IV to obtain $P_S = 48 \mu\text{C}/\text{cm}^2$. This is to be compared with the measured value¹⁸ of $50 \mu\text{C}/\text{cm}^2$. Since a 20% numerical error occurred in our earlier calculation of P_S for LiNbO_3 , we repeat in Table IV the basic data on ion shifts for this material. The result for P_S (LiNbO_3) is $60 \mu\text{C}/\text{cm}^2$, which compares favorably with the measured value¹⁸ of 71.

The second method of obtaining P_S has been described by Axe.¹⁹ Since an infrared-mode strength

depends on the square of the dynamical charge, we might expect that the strengths in Table II could be used to obtain the charges which we have only estimated above. Two major assumptions are needed in applying such a method. First, a single free-energy function must describe the crystal both above and below T_c .²⁰ Second, and probably more serious for the present case, the mode strength to be used must be measured near the transition temperature.^{19,20} Using the room-temperature strength of the lowest-frequency A_1 mode and following the method described by Axe, we obtain $P_S(\text{LiNbO}_3) = 58 \mu\text{C}/\text{cm}^2$. Since we are using slightly different values for the ion distortion for LiNbO_3 than used by Axe, we repeat his calculation to obtain $P_S(\text{LiNbO}_3) = 61 \mu\text{C}/\text{cm}^2$. Both of these values are in very reasonable agreement with the values obtained using the estimates of the effective charge shown in Table IV.

Table IV shows that an optic-mode eigenvector corresponding to the c. m. displacements listed is very similar in the two materials. This mode is also very polar and of the form to be expected from earlier discussions of the occurrence of the ferroelectric phase in LiNbO_3 .⁷

IV. CONCLUSIONS

The analysis of the infrared reflectivity of LiTaO_3 has allowed the assignment of 11 of the 13 expected fundamental-infrared and Raman-active optic modes. There are a number of weak features in the spectra which could account for the remaining two fundamentals; however, there is at present no method for making firm assignments. For both polarizations, the optic modes have sufficient strength to make the material strongly absorbing ($\alpha > 2000 \text{ cm}^{-1}$) over the entire infrared region from 100 to 900 cm^{-1} . The measured far-infrared interference spectrum has led to accurate values for the low-frequency clamped dielectric constant and its dispersion up to 70 cm^{-1} . Finally, we have shown that by assum-

TABLE IV. Prediction of ferroelectric polarization from x-ray displacements.

Ion	X-ray distortion along c axis	Displacements (c. m.)	Mass (amu)	Charge (e)
LiNbO_3 $c = 13.86 \text{ \AA}$, cell volume (2 molecules) = 105.3 \AA^3				
Li_1, Li_2	0.033c	0.513 \AA	6.94	1
Nb_1, Nb_2	0.0	0.0593 \AA	92.91	5
$\text{O}_1, \dots, \text{O}_6$	-0.08c	-0.189 \AA	16	-2
$P_S = 60 \mu\text{C}/\text{cm}^2$				
LiTaO_3 $c = 13.78 \text{ \AA}$, cell volume = 105.7 \AA^3				
Li_1, Li_2	0.028c	0.427 \AA	6.94	1
Ta_1, Ta_2	0.0	0.029 \AA	180.9	5
$\text{O}_1, \dots, \text{O}_6$	-0.145c	-0.171 \AA	16.0	-2
$P_S = 48 \mu\text{C}/\text{cm}^2$				

ing ion charges equal to the chemical valence, quite accurate values of the ferroelectric polarization can

be calculated from the ion displacements which occur at the ferroelectric phase transition.

¹B. T. Matthias and J. P. Remeika, Phys. Rev. **76**, 1886 (1949).

²P. V. Lenzo, E. H. Turner, E. G. Spencer, and A. A. Ballman, Appl. Phys. Letters **8**, 81 (1966).

³A. A. Ballman, J. Am. Ceram. Soc. **48**, 112 (1965).

⁴R. T. Denton, F. S. Chen, and A. A. Ballman, J. Appl. Phys. **38**, 1611 (1967).

⁵S. C. Abrahams and J. L. Bernstein, J. Phys. Chem. Solids **28**, 1685 (1967).

⁶S. C. Abrahams and W. C. Hamilton, J. Phys. Chem. Solids **28**, 1693 (1967).

⁷A. S. Barker and R. Loudon, Phys. Rev. **158**, 433 (1967).

⁸H. J. Levinstein, A. A. Ballman, and C. D. Capio, J. Appl. Phys. **37**, 4585 (1966).

⁹W. G. Spitzer and D. A. Kleinman, Phys. Rev. **121**, 1324 (1961).

¹⁰A. S. Barker, in *Far Infrared Properties of Solids*,

edited by S. S. Mitra and S. Nudelman (Plenum, New York, 1970).

¹¹W. L. Bond, J. Appl. Phys. **36**, 1674 (1965).

¹²I. P. Kaminow and W. D. Johnston, Jr., Phys. Rev. **160**, 519 (1967).

¹³W. D. Johnston, Jr. and I. P. Kaminow, Phys. Rev. **168**, 1045 (1968).

¹⁴A. S. Barker, Jr., Phys. Rev. **132**, 1474 (1963); **135**, 742 (1964).

¹⁵D. W. Berreman, Phys. Rev. B **1**, 381 (1970).

¹⁶D. R. Bosomworth, Appl. Phys. Letters **9**, 330 (1966).

¹⁷*Spectroscopic Techniques*, edited by D. H. Martin (North-Holland, Amsterdam, 1967), Chap. 2.

¹⁸S. H. Wemple, M. DiDomenico, Jr., and I. Camlibel, Appl. Phys. Letters **12**, 209 (1968).

¹⁹J. D. Axe, Solid State Commun. **5**, 413 (1967).

²⁰P. C. Kwok and P. B. Miller, Phys. Rev. **151**, 387 (1966).

Properties of Image-Potential-Induced Surface States of Insulators*[†]

Milton W. Cole [‡]

Department of Physics and The James Franck Institute, The University of Chicago, Chicago, Illinois 60637

(Received 6 July 1970)

The strongly repulsive interaction between electrons and He or Ne atoms, or H₂ molecules, gives rise to the existence of electronic states localized near a condensed medium consisting of such units. The attractive image potential binds the electrons weakly near the surface; the binding energy ranges from 0.4 meV for liquid He³ to 22 meV for solid D₂. Motion parallel to the surface is nearly free-electron-like. An exploration of the interaction between electrons and oscillations of the medium's surface reveals a breakdown in perturbation theory which may be remedied by correct treatment of long-wavelength oscillations. A determination is made of the temperature-dependent mobility of electrons for fields parallel to the surface. We find that the surface waves scatter more for the liquid than for the solid. A transition occurs in the mobility as the temperature increases to a point where scattering by atoms of the vapor becomes dominant over other mechanisms. A second transition occurs when the electron in the vapor becomes localized in the bubble state, and the present treatment loses its validity.

I. INTRODUCTION

This paper attempts to elaborate the characteristics of a new kind of electronic state recently proposed by Cohen and the author.¹ The electrons are localized near, but primarily external to, a condensed insulating medium which satisfies certain criteria. The media we shall discuss are composed of atoms which have a primarily repulsive interaction with electrons. Outside of the medium, the interaction is the attractive image potential. The balance between these opposing forces results in localization of excess electrons in the vicinity of the surface. Motion parallel to the surface is es-

entially unrestricted and, in fact, becomes two-dimensional in character.

The question of the existence and character of electronic surface states in general has been investigated theoretically and experimentally for nearly forty years.² Tamm³ and later Shockley⁴ showed that termination of a one-dimensional Kronig-Penney model potential of a one-dimensional crystal may yield solutions for electronic states localized near the "surface" in addition to the usual delocalized states of the bulk material. Bardeen subsequently hypothesized⁵ that surface electronic states played an important role in determining the electrostatic-potential configuration at the inter-